Available online at www.rajournals.in

RA JOURNAL OF APPLIED RESEARCH
ISSN: 2394-6709
DOI:10.31142/rajar/v5i2.05
Volume: 05 Issue: 02 February -2019

International Open Access
ICV- 74.25
Impact Factor :5.985
Page no.- 2311-2316

Modeling and Experimental Investigations of Lithium-Copper Phthalocyanine Based Cells/Batteries

Sarwan S. Sandhu[1], Clayton J. Cashion[2], Joseph P. Fellner[3]

[1,2]Department of Chemical and Materials Engineering, University of Dayton, Dayton, OH 45469
[3]Air Force Research Laboratory, Wright-Patterson Air Force Base, OH 45433

ARTICLE INFO

Publication Online:
22 February 2019

Corresponding Author:
Sarwan S. Sandhu,

ABSTRACT

Some of the basic concepts underlying electrochemical cell/battery designs are reviewed. A developed mathematical formulation is used to predict the transient dimensionless lithium concentration profiles and the transient current density and specific charge storage capacity of an active material of a cell cathode, such as copper phthalocyanine. Theoretical computational chemistry results, using Gaussian 16 software, are provided on the structure/composition of the copper phthalocyanine active material. Experimental results show the primary discharge capacity of lithium-based copper phthalocyanine coin cells at room temperature of approximately 840 mAh per gram of active material. This primary discharge capacity is more than a factor of four higher than the secondary or rechargeable capacity of commercially available lithium-ion battery cathode materials.

KEYWORDS: batteries, lithium, transient model, computational chemistry, diffusion-limited, primary, secondary

I. INTRODUCTION

The battery original concept is: A portable energy source which can be manufactured in a range of sizes. There are two categories [1] of batteries: primary (non-rechargeable) and secondary (rechargeable) batteries. An example of a primary battery is zinc-carbon battery; it contains manganese dioxide ($MnO_{2(s)}$), zinc (Zn), carbon (C), and moist zinc chloride ($ZnCl_2$) and ammonium chloride (NH_4Cl) as the cell electrolyte. The electrode half reactions and overall discharge reaction are:

Negative electrode; anodic reaction (oxidation, loss of electrons):

$$Zn \rightarrow Zn^{+2} + 2e^{-} \quad (1)$$

Positive electrode; cathodic reaction (reduction, gain of electrons):

$$2MnO_2 + 8NH_4^{+} + 2e^{-} \rightarrow 2Mn^{3+} + 4H_2O + 8NH_3 \quad (2)$$

Overall cell reaction (during cell discharge):

$$Zn + 2MnO_2 + 8NH_4^{+} \rightarrow Zn^{+2} + 2Mn^{+3} + 8NH_3 + 4H_2O \quad (3)$$

An example of a secondary battery is the lead-acid storage battery which is used in automobiles. At a state of being fully charged, this secondary battery contains one electrode made of pure lead (Pb) and the other electrode is made of lead dioxide (PbO_2). The electrolyte is sulfuric acid (H_2SO_4). In water solution H_2SO_4 dissociates into H^+ and SO_4^{2-} ions. During the discharge, the lead (Pb) electrode acts as the anode (negative electrode) and PbO_2 as the cathode (positive electrode). When an external load is placed across the electrodes, the cell provides the current, electrons leave the negative electrode and migrate through the external circuit to the positive electrode. In the cell interior, lead sulfate ($PbSO_4$), which is nearly insoluble in the electrolyte solution, is formed and deposited on both cell electrodes. When the plating of lead sulfate occurs to such a degree that the cell electrolyte cannot reach the electrode materials (Pb and PbO_2), the cell stops producing current and the cell is "dead". An independently generated current is passed through it in the opposite direction to recharge the cell. The original electrode reactions are reversed, and the electrode plates are restored to their original compositions. During the cell/battery discharge the electrode reactions are:

Negative electrode (anode reaction):

$$Pb + SO_4^{2-} \rightarrow PbSO_4 + 2e^{-} \quad (4)$$

Positive electrode (cathodic reaction):

$$PbO_2 + 4H^{+} + 2e^{-} + SO_4^{2-} \rightarrow PbSO_4 + 2H_2O \quad (5)$$

The overall cell discharge reaction:

$$Pb + PbO_2 + 2SO_4^{2-} + 4H^{+} \rightarrow 2PbSO_4 + 2H_2O \quad (6)$$

Table I shows the characteristics of commercial Li-ion battery cathode materials.

Table I. Characteristics of Commercial Li-ion Battery Cathode Materials

Material	Structure	Electric Potential vs $Li_{(s)}/Li^+$, V (average)	Specific Capacity, mAh g^{-1}	Specific Energy, Wh kg^{-1}
$LiCoO_2$	Layered	3.9	135 – 145	527 – 566
$LiNi_{0.8}Co_{0.15}Al_{0.05}O_2$ (NCA)	Layered	3.8	180 – 200	680 – 760
$LiNi_{1/3}Co_{1/3}Mn_{1/3}O_2$ (NMC)	Layered	3.8	160 – 170	610 – 650
$LiMn_2O_4$ (LMO)	Spinel	4.1	100 – 120	410 – 492
$LiFePO_4$ (LFP)	Olivine	3.45	150 – 170	518 – 587

Batteries are used in various national defense systems. Their recreational uses are in portable video game devices and music listening devices. They also find their application in: business convenient devices – laptop computers, cellular phones, pagers, calculators; safety devices – smoke detectors, emergency lighting, subway backup power; automotive starter batteries; and personal hearing aids, wristwatches, cameras, and clocks. These are some among many other uses of batteries, e.g. secondary batteries can be used to store excess electrical energy generated by the conventional electric generating power plants, wind turbines, and photovoltaic solar cells.

II. BATTERY BASICS

This section presents some of the basic concepts underlying battery design.

A. Theoretical Voltage

The theoretical voltage determination of a cell is based on its active materials, including electrode materials and electrolyte. The actual cell voltage is always less than the theoretical maximum voltage during discharge. The theoretical voltage of a cell is the sum of the reduction potential at the cathode electrode and the oxidation potential at the anode. The reduction potential at the cathode is equal to the standard reduction potential for the material in the cell cathode. The oxidation potential at the anode is equal to the negative of the standard reduction potential for the material of the cell anode. One should note that the standard potential varies if the reaction takes place in an acidic electrolyte (e.g. in a lead – acid cell) or an alkaline electrolyte (e.g. in an alkaline – manganese cell).

Example: In a lead – acid cell: $Pb_{(s)}/H_2SO_4$ in aqueous solution/PbO_2; during cell discharge:

At the anode electrode,

$$Pb + SO_4^{2-} \rightarrow PbSO_4 + 2e^-$$
$$E^{0,A} = -(-0.356V) = 0.356V\,[2]. \quad (7)$$

At the cathode electrode,

$$PbO_2 + 4H^+ + 2e^- + SO_4^{2-} \rightarrow PbSO_4 + 2H_2O$$
$$E^{0,C} = 1.685\ V\ [2] \quad (8)$$

The standard cell potential at 25 °C for the lead – acid cell is: $E^{0,cell} = (0.356 + 1.685)\ V = 2.041\ Volt$.

B. Theoretical Capacity

The theoretical specific capacity (*Ah* per *kg*) of a battery system is calculated on the basis of only the active materials of the battery electrodes which participate in the overall cell reaction. It is obtained by dividing the electrochemical equivalence of the cell anode and cathode. For the lead – acid cell: $Pb_{(s)}/H_2SO_4$ in aqueous solution/PbO_2, as shown in Eq. (4) and Eq. (5), 2 g-equivalents = 2*F* of charge is involved; i.e this much charge flows through an external load per g-mole of occurrence of the overall cell reaction, Eq. (6). So, theoretical capacity of this reaction is = 2*F*/(mass of the active materials involved) = $2F/(m_{Pb}+m_{PbO2})$ = 120.09 *Ah/kg*, where *F* [=] Faraday constant = 96487.0 coulomb per g-equivalent and m_i = molecular weight of an active electrode species. Note that the capacity of a cell is expressed in terms of current flow from an electrochemical cell reaction over time. It is defined as the product of current (amperes) and time (*h*). An electrochemical cell which can sustain one ampere of current for three hours has the same capacity as a cell which can sustain three amperes of current for one hour; i.e. capacity = three ampere – hour (3 *Ah*).

Theoretical capacity of a cell/battery can also be expressed on an energy (watt-hour) basis by multiplying the theoretical cell voltage and charge (Ah):

$$Energy(Wh) = [Voltage(V)] \times [Capacity(Ah)] \quad (9)$$

The cell energy density per unit of cell active material mass is calculated by multiplication of the theoretical voltage (*V*) by the theoretical specific charge capacity (*Ah/kg*):

$$Specific\ energy\ density\left(\frac{Wh}{kg}\right) = [Voltage(V)] \times \left[Specific\ charge\ capacity\left(\frac{Ah}{kg}\right)\right] \quad (10)$$

For example, for the lead–acid battery theoretical specific energy density at 25 °C = (2.041*V*)(120.09 *Ah/kg*) = 244.92

(*Wh/kg*). Specific energy density is a useful measure for comparison of different battery technologies.

C. Actual Capacity

The actual energy density of a battery in (*Wh/kg*) can be as low as, for example, 10–20 percent of the theoretical capacity. This is because the added mass from required but nonreactive materials; such as containers, separators, and electrolyte; used in construction of a battery.

It is conventional to state the available capacity of a battery at a particular discharge rate and battery temperature with the assumption of a constant discharge rate (current). The 20–hour rate at 20 °C is commonly used. If a battery discharges continuously at 20 °C and takes 20 hours to reach its discharge voltage cutoff; then, its "nominal capacity" is referred to as: C_{20}. Capacity of a cell is not the same for all discharge rates because the capacity of a battery, in general, decreases with increasing discharge current.

Example:

A battery discharging at a rate of 0.1 *A* takes 20 hours to reach the discharge voltage cutoff. What is the C_{20} values? If a battery with this C_{20} capacity were to be discharged at a rate of 0.4 *A*, how many hours would it be expected to last?

Solution:

C_{20} = (0.1*A*)(20h) = 2 *Ah*. Time for a full discharge at 0.4 *A* rate = (C_{20})/(0.4 *A*) = (2 *Ah*)/(0.4 *A*) = 5 *hours*. Actually, the battery would last less than 5 hours because battery capacity typically decreases with an increase in discharge current.

III. FORMULATION AND MODELING

A. Formulation

A typical coin cell used in our experiments is illustrated in Figure 1 below. The coin cell consisted of lithium foil as the anode, Celgard 2300 as the separator, 1 molar lithium bis (fluorosulfonyl) imide (LiFSI) in dimethoxymethane (DME) as the electrolyte, and 60wt% CuPc (purity greater than 99%) as the cathode active material with 30 wt% carbon black as the cathode electronic conductor and 10 wt% PVDF as the cathode binder.

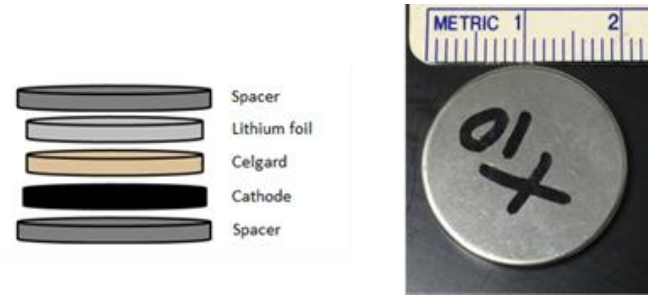

Figure 1: Lithium-foil based coin cell.

To provide insight into the mechanistic processes governing the performance behavior of a lithium – based cell: $Li_{(s)}$/electrolyte/cathode electrode active containing active material such as copper phthalocyanine ($CuPc_{(s)}$) or iron phthalocyanine ($FePc_{(s)}$), the process modeling activity has been continued since 2015 [3–6]. Our experimental and theoretical efforts in research and development of the lithium–based cell cathode electrode with $CuPc_{(s)}$ or $FePc_{(s)}$ as the cathode active material have led us to conclude that the lithium-ion diffusion in the cathode active material and electronic conductance are the major processes controlling the overall cell discharge behavior. Here it is assumed that the electronic conductance of a composite cathode (composed of nanometer scale active material grains and electronic conductive material particles such as graphene particles) in contact with an electrolyte is faster than lithium-ion diffusion inside the cathode active material grain.

Here, the lithium-ion diffusion in the solid-state cathode active material, $CuPc_{(s)}$, in the lithium–based cell cathode of slab geometry shown in Figure 2 is being modelled. Transport of lithium ions in the active material, via configurational diffusion [7], is assumed to be one dimensional from y = L plane, the interface between the cell electrolyte and the cathode active material, towards the current collector at the y = 0 plane during the cell discharge period. All other faces perpendicular to x- and z-coordinates are assumed to be electrically insulated from the electrolyte. The lithium–ion transport in the cell electrolyte, lithium ion charge transfer across the interface between the electrolyte and cathode active material, and subsequently adjustment of lithium ions in the active material to occupy the most suitable active sites (to satisfy the condition of minimum Gibbs free energy for the structural stability of the cathode active material) are assumed to be very rapid relative to the lithium ion transport via the configurational diffusion in the active material channels of very narrow width, 2.5 – 3.5 Å. The transient mole balance [6] for lithium ions over the spatial element of thickness, Δy, shown in Figure 2 leads to:

$$\frac{\partial C}{\partial t} = \bar{D}_e \frac{\partial^2 C}{\partial y^2} \tag{11}$$

where C = lithium ion concentration in the active material at y–location, $\bar{D}_e$ = concentration mean effective diffusivity of lithium ions in the active material $= \dfrac{\int_{C_0}^{C^S} D_e\, dC}{C^S - C_0}$, C^S = lithium ion concentration in the active material at y = L plane, C_0 = initial concentration of lithium ions in the active material, y = distance measured from the interface between the cathode active material and the current collector at the y = 0 plane as shown in Figure 2, and t = time. To solve the partial differential equation (PDE), Eq. (11) the initial and suitable spatial boundary conditions are:

$$I.C.: \quad C(y,0) = C_0, \quad 0 < y < L \tag{12}$$

$$B.C.1: \quad \frac{\partial C(0,t)}{\partial y} = 0, \quad t > 0 \tag{13}$$

$$B.C.2: \quad C(L,t) = C^s, \quad t > 0 \tag{14}$$

For mathematical convenience, the following dimensionless dependent and independent variables are introduced into the PDE, Eq. (11) as well as into the initial and boundary conditions.

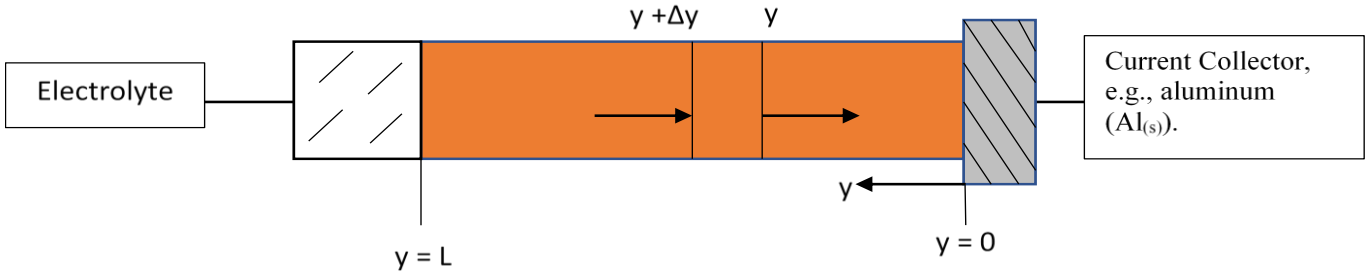

Figure 2: Slab type cathode active material electrode in contact with the cell electrolyte.

$$\psi = \frac{C^s - C}{C^s - C_0}\ ,\ \zeta = \frac{y}{L},\ and\ \tau = \frac{\bar{D}_e t}{L} \tag{15}$$

The resulting PDE and the initial and boundary conditions are:

$$\frac{\partial \psi}{\partial \tau} = \frac{\partial^2 \psi}{\partial \zeta^2} \tag{16}$$

$$I.C.: \quad \psi(\zeta, 0) = 1, \quad 0 < \zeta < 1 \tag{17}$$

$$B.C.1: \quad \frac{\partial \psi(0,\tau)}{\partial \zeta} = 0, \quad \tau > 0 \tag{18}$$

$$B.C.2: \quad \psi(1,\tau) = 0 \quad \tau > 0 \tag{19}$$

Using the method of separation of variables, the PDE, Eq. (16), has been solved in conjunction with the conditions, Eqs. (17) through (19) [7]. Only the main conceptual steps and formulated equations are provided here. The reader is referred to the reference [7] for the formulation detail. The solution of the PDE, Eq. (16), is:

$$\psi = \frac{4}{\pi}\sum_{n=0}^{n=\infty}\frac{(-1)^n}{(2n+1)}\cos\left[\left(n+\frac{1}{2}\right)\pi\zeta\right]e^{-\left[\left(n+\frac{1}{2}\right)\pi\right]^2\tau} \tag{20}$$

Equation (20) quantitatively describes the dimensionless quantity ψ representing the local lithium concentration in the cathode active material differing from that at y = L location as a function of both dimensionless spatial distance, ζ, and the dimensionless time, τ. The series solution, Eq. (20), converges rapidly for large values of τ. For small τ values, the convergence is slow. At a fixed τ value, ψ as a function of ζ can be calculated and plotted. Such plots of ψ vs ζ at various τ values are thus made available for their practical applications. Additional derived formulas [8] are:

Lithium ion molar flux, $\left[\frac{mol\ Li}{cm_s^2\ s}\right]$, at $\zeta = \left(\frac{y}{L}\right) = 1$,

$$-\dot{N}\Big|_{\zeta=1} = -\dot{N}_1 = 2\bar{D}_e\left[\frac{C^s - C_0}{L}\right]\times \left(\sum_{n=0}^{n=\infty}(-1)^n \sin\left[\left(n+\frac{1}{2}\right)\pi\right]e^{-\left[\left(n+\frac{1}{2}\right)\pi\right]^2\tau}\right) \tag{21}$$

The instantaneous current density, $\left[\frac{A}{cm_s^2}\right]$, at the cell electrolyte-cathode electrode active material interface (controlled by the lithium ion diffusion in the cathode active material),

$$i_s = \left(-\dot{N}_1\right)F = \left[\frac{2\bar{D}_e\left(C^s - C_0\right)F}{L}\right]\times \left(\sum_{n=0}^{n=\infty}(-1)^n \sin\left[\left(n+\frac{1}{2}\right)\pi\right]e^{-\left[\left(n+\frac{1}{2}\right)\pi\right]^2\tau}\right) \tag{22}$$

where F = Faraday constant = 96487 C per g-equivalent. Specific charge stored in the cathode active material, $\left[\frac{mAh}{g_{active}}\right]$, during the cell discharge period, τ;

$$q_{ch} = \left[\frac{0.2252\left(C^s - C_0\right)F}{\rho_{active}}\right]\times \left\{\sum_{n=0}^{n=\infty}\frac{(-1)^n}{(2n+1)^2}\sin\left[\left(n+\frac{1}{2}\right)\pi\right]\left[1-e^{-\left[\left(n+\frac{1}{2}\right)\pi\right]^2\tau}\right]\right\} \tag{23}$$

where ρ_{active} = density of the active material. Equation (23) can also be re-expressed as the specific molar charge capacity, $\left[\frac{mAh}{mol\ Li}\right]$:

$$q_{ch,sp} = \frac{q_{ch}\,\rho_{active}}{\left(C^s - C_0\right)} = 0.2252(F)\times \left\{\sum_{n=0}^{n=\infty}\frac{(-1)^n}{(2n+1)^2}\sin\left[\left(n+\frac{1}{2}\right)\pi\right]\left[1-e^{-\left[\left(n+\frac{1}{2}\right)\pi\right]^2\tau}\right]\right\} \tag{24}$$

1) *Discussion of Computed/Plotted Data*: Figure 3 shows the plots of $\psi = \frac{C^s - C}{C^s - C_0}$ versus $\zeta = \frac{y}{L}$ at a number of $\tau = \left(\frac{\bar{D}_e t}{L^2}\right)$ values.

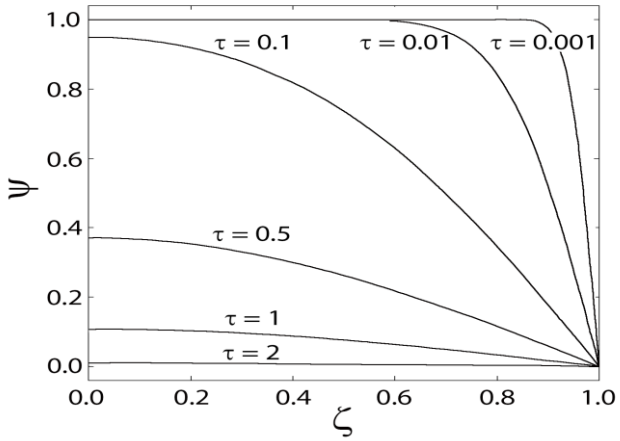

Figure 3: Dimensionless concentration, ψ, versus dimensionless position, ζ, at different dimensionless time values, τ.

At each τ value, the dimensionless concentration difference, ψ, increases from its value of 0.0 at $\zeta = 1$ (the electrolyte-solid cathode active material interface) to a transient value of ψ at $\zeta = 0$ (the solid cathode active material–solid current collector interface shown in Figure 2). As the dimensionless time, τ, increases; the ψ vs. ζ profile moves downwards toward the limiting profile at $\tau > 2$. At this dimensionless time, ψ is approximately 0 everywhere. This implies that the lithium concentration, C, has reached C^S level at this dimensionless time, $\tau > 2$.

In Figure 4, the dimensionless current density, $i_{s,d} = \left(\frac{i_s L}{\bar{D}_e \left(C^S - C_0\right) F}\right)$, is observed to decrease rapidly as τ increases.

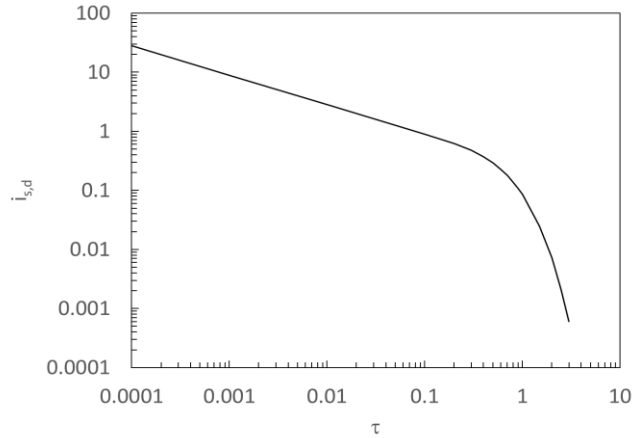

Figure 4: Dimensionless current density vs dimensionless time.

During the cell discharge period, as τ increases, the fraction of active sites in the cathode active material occupied by the intercalated lithium increases. This results in lowering of the lithium ion concentration gradient at $\zeta = 1$; consequently, in lowering of the lithium ion molar flux and the current density. For $\tau > 2$, $i_{s,d} \approx 0$.

Figure 5 shows the specific charge storage, $q_{ch,sp}$, in the cathode active material versus dimensionless time, τ.

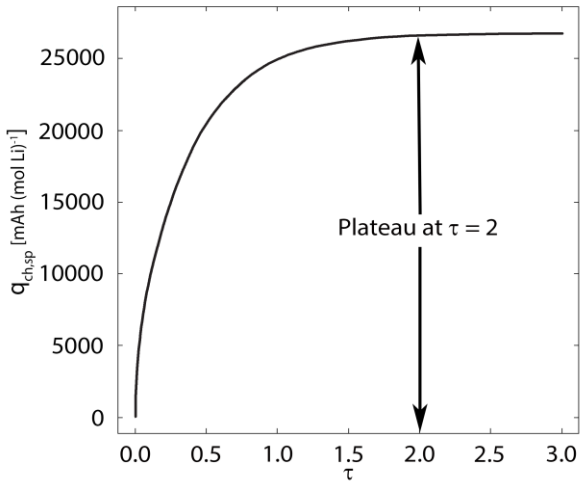

Figure 5: Specific charge storage capacity per mole of lithium vs dimensionless time, τ.

As τ increases, $q_{ch,sp}$ increases. It plateaus around $\tau = 2$. Beyond $\tau = 2.0$, the change in $q_{ch,sp}$ is negligibly small.

B. The Gaussian-based Computational Work on Copper Phthalocyanine

Table II shows the open-circuit cell voltages for lithium intercalation into copper phthalocyanine ($CuPc_{(s)}$) for up to four lithium atoms per molecule of CuPc. Theoretical Gibbs free energy was determined using the Gaussian 16 software package. The Heyd–Scuseria-Ernzerhof functional, HSEHIPBE, with 6-31 + G(d,p) basis set was used on C, H, N, Li atoms and the basis set aug–cc–pvdz on the Cu atom. The simulation also included the effect of lithium ions in the diethoxyethane (DEE) solvent using the Polarizable Continuum Model (PCM). As shown in Table 2, the calculated cell voltage ranges from 1.5 to 2.0 volts. The experimentally observed cell voltages at very low currents, such as the C/100 rate, are close to the voltages in the voltage range shown in Table 2.

Table II: Calculated cell voltage at 298.15 K using the Gaussian 16.

Species (lowest energy)	Calculated Cell Voltage (V)
Li_2CuPc (doublet)	1.797
Li_3CuPc (triplet)	1.611
Li_4CuPc (doublet)	1.505

The open-circuit cell voltages in Table 2 correspond to optimized geometrical configurations of Li_xCuPc molecule. An example of an optimized configuration of Li_2CuPc molecule is shown in Figure 6. The side view on the right shows some, but minimal, distortion of the normally planar molecular structure.

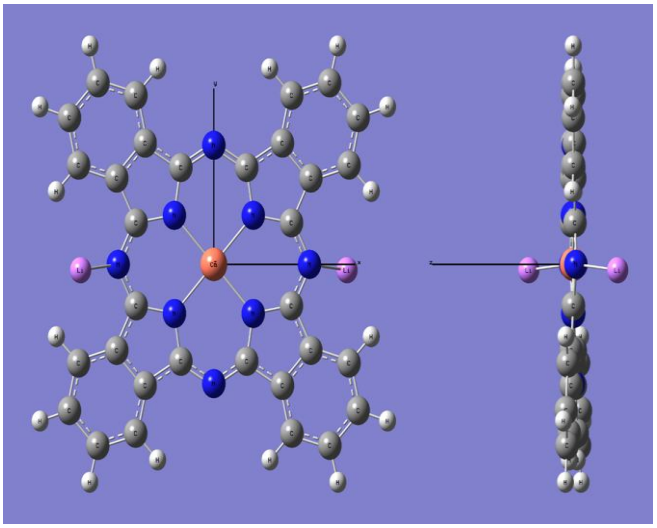

Figure 6: Optimized geometrical configuration of Li_2CuPc molecule using Gaussian 16 (top and side views).

IV. EXPERIMENTAL

Figure 7 shows the discharge of a lithium/$CuPc_{(s)}$ coin cell at 20 °C. The cell is first discharged at the C/10 rate to the cut-off voltage of 1.0 V. It is then placed on open-circuit for two hours. To determine the remaining residual capacity, it is discharge at the low rate of C/96 to 1.0-volt cut-off. For this cell configuration, a capacity of about 550 mAh g^{-1} is observed at the C/10 discharge rate. If the residual capacity is included, the total capacity is about 840 mAh g^{-1} of $CuPc_{(s)}$.

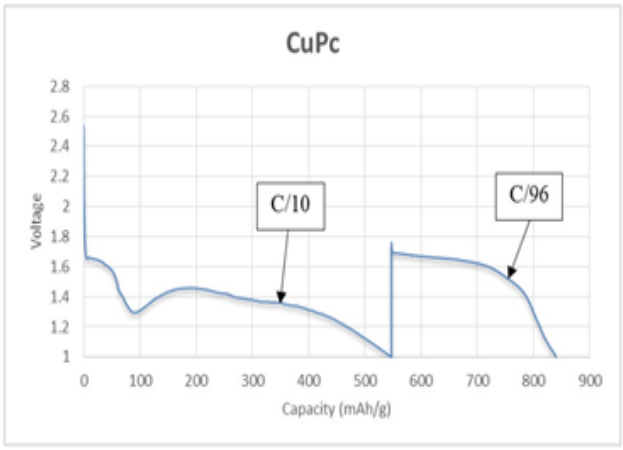

Figure 7: Coin cell discharge curve of 60 wt% CuPc with 30 wt% carbon black and 10 wt% PVDF.

V. CONCLUSIONS

The developed formulation presented in this paper predicts the transient profiles of the dimensionless lithium ion concentration versus the dimensionless distance in a cathode active material such as copper phthalocyanine. The formulation also predicts the dimensionless current density and specific charge storage capacity versus the dimensionless time.

The cell open-circuit voltage estimates obtained using the Gaussian 16 software package at 25 °C are quite close to those observed experimentally at very low current densities such as C/100. The presented experimental $Li_{(s)}/CuPc_{(s)}$ coin cell discharge data at 20 °C shows the charge storage capacity of about 840 mAh g^{-1} of CuPc at the cell cut-off voltage of 1 volt. This capacity is much higher than 120, 148, 200, and 170 mAh g^{-1} of $LiMn_2O_{4(s)}$, $LiCoO_{2(s)}$, $LiNi_{0.8}Co_{0.15}Al_{0.05}O_{2(s)}$, and $LiFePO_{4(s)}$ used as the cathode active material in the rechargeable lithium-ion batteries, respectively.

REFERENCES

1. Rubin, E.S. (2001), Introduction to Engineering and the Environment, Chapter 4, p.128, McGraw-Hill Companies, Inc., New York, NY 10020.
2. Prentice, G. (1991), Electrochemical Engineering Principles, p.271, Prentice-Hall Inc.
3. Sandhu, S.S., Fellner, J.P. (2015), J. Chem. Eng. Process Technol., 6, 257
4. Sandhu, S.S., Fellner, J.P., Tzao, M., Cashion, C.J. (2017), International Journal of Engineering Technology Management and Applied Sciences (IJETAS), 5 , 24.
5. Sandhu, S.S., Fellner, J.P., Dudi, S.P. (2017), Current Topics in Electrochemistry, 19, 91.
6. Froment, G.F., Bischoff, K.B., Wilde, J. De. (2011) Chemical Reactor Analysis and Design (3rd Edition). John Wiley & Sons, Inc. pp. 64 – 75, 173.
7. Bird, R.B., Stewart, W.E, Lightfoot, E.N. (2007), Transport Phenomena (revised second edition), John Wiley & Sons, Chapters 18 and 19.
8. Sandhu, S.S. (2018), The U.S. Air Force 2018 SFFP (Summer Faculty Fellowship Program) Technical Report, Air Force Research Laboratory Publication number (to be assigned), Wright – Patterson Air Force Base, OH 45433.